SPANDIDOS PUBLICATIONS

INTERNATIONAL JOURNAL OF MOLECULAR MEDICINE 46: 427-438, 2020

Promotion of liver regeneration and anti-fibrotic effects of the TGF-β receptor kinase inhibitor galunisertib in CCl_4-treated mice

ATSUTAKA MASUDA[1,2], TORU NAKAMURA[1,2], MITSUHIKO ABE[1,2], HIDEKI IWAMOTO[1,2], TAKAHIKO SAKAUE[1,2], TOSHIMITSU TANAKA[1,2], HIROYUKI SUZUKI[1,2], HIRONORI KOGA[1,2] and TAKUJI TORIMURA[1,2]

[1]Division of Gastroenterology, Department of Medicine, School of Medicine, Kurume University; [2]Liver Cancer Research Division, Research Center for Innovative Cancer Therapy, Kurume University, Kurume, Fukuoka 830-0011, Japan

Received November 8, 2019; Accepted March 30, 2020

DOI: 10.3892/ijmm.2020.4594

Abstract. The cytokine transforming growth factor-β (TGF-β) serves a key role in hepatic fibrosis and has cytostatic effects on hepatocytes. The present study investigated the anti-fibrogenic and regenerative effects of the TGF-β receptor type I kinase inhibitor galunisertib (LY2157299) in mice with carbon tetrachloride (CCl_4)-induced liver cirrhosis and *in vitro*. Mice were intraperitoneally treated with CCl_4 for 8 weeks. At week 5, the mice were divided randomly into four treatment groups: Vehicle-treated; and treated with low-; middle-; and high-dose galunisertib, which was administered from weeks 5-8. The mice were sacrificed after 8 weeks of CCl_4 treatment. Liver fibrosis, as evaluated by histology and determination of hydroxyproline content, progressed during week 4-8 of CCl_4 treatment in the vehicle-treated mice. Galunisertib treatment dose-dependently prevented liver fibrosis, as demonstrated by the direct inhibition of α-smooth muscle actin-positive activated hepatic stellate cells (HSCs) after 8 weeks of CCl_4 treatment. The levels of active matrix metalloproteinase (MMP)-9 in galunisertib-treated livers were significantly increased compared with the vehicle-treated livers. In the high-dose group, the number of PCNA-positive hepatocytes and endothelial cells markedly increased compared with the vehicle group. Reverse transcription-quantitative PCR analysis verified that interleukin-6 and epiregulin expression levels were significantly increased in livers from the group treated with high-dose galunisertib compared with the vehicle-treated group. Galunisertib inhibited the proliferation of activated HSCs and collagen synthesis in addition to restoring MMP activity. Moreover, galunisertib promoted liver remodeling by proliferating hepatocytes and vascular endothelial cells, while significantly increasing liver weight. These results are consistent with the cytostatic action of TGF-β that negatively regulates liver regeneration, and demonstrated that galunisertib inhibited TGF-β signaling, halted liver fibrosis progression and promoted hepatic regeneration. The results of the present study suggest that galunisertib may be an effective treatment for liver cirrhosis.

Correspondence to: Dr Toru Nakamura, Division of Gastroenterology, Department of Medicine, School of Medicine, Kurume University, 67 Asahi-machi, Kurume, Fukuoka 830-0011, Japan
E-mail: ntoru@med.kurume-u.ac.jp

Key words: galunisertib, hepatic regeneration, liver fibrosis, matrix metalloproteinase, Smad, transforming growth factor-β inhibition

Introduction

Liver fibrosis results from chronic liver injury, for example persistent hepatitis virus infection, excessive alcohol intake, non-alcoholic steatohepatitis, autoimmune disorders, intrahepatic cholestasis, drug abuse and metabolic abnormalities. Accumulation of excessive extracellular matrix (ECM) proteins leads to liver cirrhosis (LC), which is a leading cause of morbidity and mortality worldwide (1). Furthermore, progression of cirrhotic stage liver disease frequently occurs with hepatocellular carcinoma (HCC) (2,3). Therefore, anti-fibrotic therapies are urgently required to decrease the mortality associated with liver injury and HCC.

There are ~140 clinical anti-fibrotic trials currently registered at ClinicalTrials.gov (http://clinicaltrials.gov). To develop an effective anti-fibrotic agent, an understanding of the precise mechanism involved in liver fibrosis progression is required. Transforming growth factor-β (TGF-β) is generally considered to be a key cytokine in hepatic fibrosis and an inhibitor of hepatocyte growth (4,5). TGF-β is also the most potent stimulus for the synthesis of type-I collagen and other matrix constituents. Therefore, agents that could inhibit the action of TGF-β would contribute to suppression of liver fibrosis by lowering levels of circulating TGF-β, antagonizing its receptors, and/or blocking its activation via intracellular signaling pathways. We previously reported that the inhibition of TGF-β signaling using adenovirus-mediated transfer

of a mutated TGF-β receptor gene to rats with dimethylnitrosamine-induced liver injury prevented the progression of liver fibrosis and promotes hepatic regeneration (6-8). Our results suggested that anti-TGF-β agents, i.e., serine/threonine kinase inhibitors, antibodies, antisense or fusion proteins of TGF-β receptors, may be a potentially effective therapy for liver fibrosis; however, there are no specific inhibitors of TGF-β signaling being tested in clinical settings to date.

TGF-β is also involved in the progression and metastasis of cancer. The anti-tumor action of TGF-β signaling inhibitors, including galunisertib, has attracted significant attention and is being tested in clinical trials (9). Galunisertib is a small-molecule inhibitor that targets the TGF-β receptor type-I kinase (10). This agent demonstrates potent and selective inhibition of TGF-β receptor type-I and also affects downstream signaling by inhibiting Smad phosphorylation (11). More recently, a Phase Ib study involving Japanese patients with unresectable HCC (NCT02240433) assessed the safety and anti-tumor potential of galunisertib in combination with the receptor tyrosine kinase inhibitor sorafenib (12). Galunisertib also demonstrated significant antifibrotic potency in a human *ex vivo* model using precision-cut liver sections from both healthy controls and patients with cirrhosis (13). To examine the potential therapeutic application of galunisertib for the treatment of liver fibrosis, the present study investigated the anti-fibrogenic and regenerative effects of galunisertib on liver cirrhosis induced by carbon tetrachloride (CCl_4) in mice.

Materials and methods

Cell lines and culture conditions. The immortalized human hepatic stellate cell (HSC) line LX-2 was purchased from EMD Millipore Corporation (EMD Millipore), the human hepatoblastoma HepG2 cell line was purchased from Cellular Engineering Technologies (Cellular Engineering Technologies Inc.), and human umbilical vein endothelial cells (HUVEC) were purchased from PromoCell GmbH. LX-2 and HepG2 cells were cultured in DMEM (Wako Pure Chemical Industries, Ltd.) supplemented with 10% FBS (Biowest SAS). HUVECs were cultured in EGM2 (Lonza Group, Ltd.) lacking hydrocortisone and supplemented with 5% FBS, growth factors [human fibroblast growth factor β (hFGFβ), human vascular endothelial growth factor (hVEGF), human insulin-like growth factor-1 (hIGF-1) and human epidermal growth factor (hEGF)], penicillin (100 U/ml) and streptomycin (100 μg/ml; Nacalai Tesque, Inc.) in a humidified atmosphere containing 5% CO_2 at 37˚C.

To evaluate the effect of galunisertib on LX-2 cells using reverse transcription-quantitative (RT-q) PCR and western blot analysis, the cells were cultured under serum-starved conditions at 37˚C overnight and then treated with the indicated concentration of galunisertib (20, 200 and 2,000 nM) or vehicle under stimulation with 5 ng/ml TGF-β1 (R&D Systems, Inc.) for 2 and 48 h for the western blot analysis and RT-qPCR assays, respectively. Galunisertib was dissolved in dimethyl sulfoxide (DMSO) and diluted with culture medium.

Cell proliferation assay. HepG2 cells, LX-2 cells and HUVECs were plated onto uncoated 96-well plates at a density of $1x10^3$ cells/well for HepG2 and HUVEC or $3x10^3$ cells/well for LX-2 and cultured for 24 h. After overnight at 37˚C incubation in serum-free medium, the medium was changed to medium containing 10% FBS for HepG2 cells, serum-free medium for LX-2 cells, or EGM2 medium supplemented with growth factors (hFGFβ, hVEGF, hIGF-1 and hEGF) and 5% FBS for HUVEC. The indicated concentrations of galunisertib and human TGF-β1 (5 ng/ml) were then added to the culture media. The cells were incubated for another 2, 3 or 5 days for LX-2, HepG2 or HUVEC cells, respectively. Cell proliferation rates were determined using Cell Count Reagent SF (Nacalai Tesque, Inc.) according to the manufacturer's protocol.

Tube formation assay. Tube formation assays were performed using a μ-slide angiogenesis kit (ibidi GmbH) according to the manufacturer's protocol. Chilled liquid Matrigel was applied to the inner wells of a μ-slide (10 μl per well) and allowed to solidify for 1 h at 37˚C. HUVECs were suspended at a density of $1x10^3$ cells/μl with EGM2 medium containing several growth factors (hFGFβ, hVEGF, hIGF-1 and hEGF) and 10% FBS with or without galunisertib (2,000 nM) and TGF-β1 (5 ng/ml). Cell suspensions (50 μl) were applied into the upper well of the μ-slide and incubated at 37˚C for 16 h prior to staining with Calcein AM (5 μg/ml; PromoCell GmbH) at 37˚C for 15 min and capture using the BZ-X 710 computer-assisted inverted light microscope (Keyence Corporation) at magnification, x2. The cavities were counted using computer-assisted image software (Adobe Photoshop CC 2017 version 18.1.1; Adobe Systems, Inc.).

Animal model. Male C57BL/6 mice (6-week-old) were purchased from Japan SLC, Inc. Mice were maintained at room temperature (21±2˚C) with a 12:12 h dark: light cycle and had *ad libitum* access to food (standard laboratory chow) and water. The experimental protocol was approved by the Ethics Review Committee for Animal Experimentation of the Kurume University School of Medicine.

Experimental conditions and administration of galunisertib. Galunisertib was provided by Eli Lilly and Company. Liver fibrosis was induced by CCl_4 (Wako Pure Chemical Industries; 1 μl/g BW in olive oil) that was administered to mice intraperitoneally under inhalational anesthesia using 3% isoflurane (Wako Pure Chemical Industries) twice a week for 8 weeks. Following the procedure, breathing and changes in circulation once a day were checked by appearance, and one of mice in vehicle-treated group was euthanized by cervical dislocation under 3% isoflurane anesthesia due to intestinal rupture. In week 5, the mice were divided randomly into four treatment groups: Vehicle-treated (vehicle group; n=7) and treated with low-(50 mg/kg/day; n=7) middle-(150 mg/kg/day; n=7) and high-dose (300 mg/kg/day; n=4) galunisertib, which was administered by oral gavage twice daily from week 5 to week 8. The vehicle group received the control mixture (1 w/v% carboxymethylcellulose, 0.5 w/v% sodium lauryl sulfate and 0.085 w/v% povidone) without galunisertib. CCl_4 administration was continued twice weekly until week 8. Mice in the intact group (n=4) were intraperitoneally injected with olive oil alone and orally received the control mixture without galunisertib. On day 56, 72 h after the final CCl_4 injection, ~800 μl of whole blood samples were obtained from inferior vena cava

under 3% isoflurane inhalational anesthesia. Mice were euthanized by cervical dislocation under 3% isoflurane anesthesia. Following euthanasia, whole liver samples were collected for histological and molecular analyses.

RT-qPCR. Total RNA was extracted using an Isogen kit (Nippon Gene Co., Ltd) following the manufacturer's protocol. Single-strand cDNA was synthesized using a high-capacity RNA-to-cDNA kit (Applied Biosystems; Thermo Fisher Scientific, Inc.). qRT-PCR was performed using TaqMan® Universal Master Mix (Applied Biosystems; Thermo Fisher Scientific, Inc.) with technical triplicates using a StepOnePlus™ Real-Time PCR System (Applied Biosystems; Thermo Fisher Scientific, Inc.). The thermocycling parameters were as follows: 2 min at 50˚C and 10 min at 95˚C, followed by 45 cycles of 15 sec at 95˚C and 1 min at 60˚C. Relative quantification of gene expression was performed according to the $2^{-\Delta\Delta Cq}$ method (14) using StepOne Software 2.0 (Applied Biosystems; Thermo Fisher Scientific, Inc.), and *Gapdh* (as a housekeeping gene in mice) or *GAPDH* (as a housekeeping gene in human) was used as the reference for normalization of the results. Primer sequences are listed in Table SI.

The expression of genes involved in liver regeneration was analyzed by PCR array using a Mouse Growth Factors RT^2 Profiler PCR Array Plate (cat. no. PAMM-041Z; Qiagen, Inc.) and the StepOnePlus™ Real-Time PCR System according to the manufacturer's protocol. The data were analyzed using SDS Software 2.3 and RT^2 Profiler PCR Array Data Analysis version 3.5 (www.sabiosciences.com/pcrarraydataanalysis.php; SABiosciences Corporation; Qiagen, Inc.). Gene expression was normalized to the mean of house-keeping genes in the array.

Histological examination. The liver tissues fixed in 10% buffered formalin for 24 h at room temperature were embedded in paraffin and sliced to form 5 μm-thick sections. The sections were either processed using Mallory's Azan staining using 0.1% azocarmine G (cat. no. 1A266; Waldeck, Division Chroma) for 50 min at 60˚C and Aniline Blue-Orange G (cat. no. 4005-2; Muto Pure Chemicals co., LTD.) for 15 min at room temperature, or were analyzed histochemically using antibodies against α-smooth muscle actin (α-SMA; cat. no. 19245; 1:1,000; Cell Signaling Technology, Inc.), proliferating cell nuclear antigen (PCNA; cat. no. sc-7907; 1:300; Santa Cruz Biotechnology), cleaved caspase-3 (cat. no. 9664; 1:50; Cell Signaling Technology, Inc.) and FITC conjugated isolectin B4 (cat. no. FL-1201; 1:300; Vector Laboratories, Inc.). The tissues were incubated with primary antibodies overnight at 4˚C. Immunoreactivity was visualized using EnVision+ system HRP labelled polymer anti-rabbit (cat. no. K4003; Dako; Agilent Technologies, Inc.) for 30 min at room temperature and a DAB commercial kit (Liquid DAB+ Substrate Chromogen System; cat. no. K3468; Dako; Agilent Technologies, Inc.). For double-immunofluorescence examination, slides were incubated with Alexa Fluor 568-conjugated anti-rabbit IgG (cat. no. A11036; 1:200; Invitrogen; Thermo Fisher Scientific, Inc.) for 30 min at room temperature and mounted with DAPI (VECTASHIELD mounting medium with DAPI; cat. no. H1200; Vector Laboratories, Inc.) to label the nuclei. Apoptosis was detected by modifying DNA fragments using terminal deoxynucleotidyl transferase mediated d-UTP nick end labeling (TUNEL) staining. Digoxigenin-labeled UTP was detected with an antibody to digoxigenin. An *in situ* apoptosis detection kit (cat. no. S7101; EMD Millipore) was used for TUNEL staining according to the manufacturer's protocol. In brief, the tissue sections were pretreated with proteinase K (20 μg/ml; Wako Pure Chemical Industries, Ltd.) for 15 min at room temperature. Following washing with distilled water for 3 min trice, 3% hydrogen peroxide (Wako Pure Chemical Industries, Ltd.) was used to quench endogenous peroxidase for 5 min at room temperature. The sections were incubated with Working Strength TdT Enzyme (EMD Millipore) for 1 h at 37˚C, followed by Stop/Wash buffer (EMD Millipore) for 10 min at room temperature. Immunoreactivity was visualized using Anti-Digoxigenin Conjugate (EMD Millipore) for 30 min at room temperature and Peroxidase Substrate (EMD Millipore). The nuclei were stained with hematoxylin for 30 sec at room temperature. Blue-stained areas in Mallory's Azan staining, the immunoreactive areas for α-SMA, and PCNA-, TUNEL- and cleaved caspase-3-positive hepatocytes were identified with computer-assisted image software (Adobe Photoshop CC 2017 version 18.1.1) by a technician who was blinded to the treatment regimens. The proliferation/apoptosis (PA) index was calculated by % PCNA-positive hepatocytes/% TUNEL-positive hepatocytes. A total of two fields were assessed at magnification, x10 for each sample for the Mallory's Azan and α-SMA staining. For the PCNA, TUNEL and cleaved caspase-3 analysis of each sample, a total of five fields were assessed at magnification, x40.

Western blot analysis. Frozen liver tissues were homogenized in RIPA buffer (Thermo Fisher Scientific, Inc.) containing 1% protease inhibitor cocktail (Sigma-Aldrich; Merck KGaA) and 1% phosphatase inhibitor cocktail (ready-made; Thermo Fisher Scientific, Inc.). The protein concentration was determined using a detergent compatible protein assay kit (Bio-Rad Laboratories, Inc.). Equal amounts of 20 μg protein per lane were loaded onto 10% SDS-PAGE, electrophoresed, and electrotransferred to a FluoroTrans membrane (Pall Life Sciences). Following protein transfer, the membranes were blocked with 2% skimmed milk (Cell Signaling Technology, Inc.) for 1 h at room temperature and incubated overnight at 4˚C with primary antibody [antibodies against phosphorylated (p-)Smad2 (cat. no. 3101; 1:1,000), total (t-)Smad2 (cat. no. 5339; 1:1,000), p-Smad3 (cat. no. 9520; 1:1,000), t-Smad3 (cat. no. 9523; 1:1,000), Smad4 (cat. no. 9515; 1:1,000), p-p38 mitogen-activated protein kinase (MAPK; cat. no. 9216; 1:2,000), t-p38 MAPK (cat. no. 9212; 1:1,000), p-extracellular signal-regulated kinase (ERK)1/2 (cat. no. 4377; 1:1,000) and t-ERK1/2 (cat. no. 4695; 1:1,000) were from Cell Signaling Technology, Inc.; antibodies for matrix metalloproteinase (MMP)-1 (cat. no. ab137332; 1:1,000) and MMP-13 (cat. no. ab39012; 1:3,000) were from Abcam; antibodies for PCNA (cat. no. sc71858; 1:1,000) and GAPDH (cat. no. sc25778; 1:1,000) were from Santa Cruz Biotechnology]. Visualization of protein signals was achieved with a HRP-conjugated secondary antibodies [anti-rabbit IgG, HRP-conjugated whole ab donkey (cat. no. NA934; 1:10,000; GE Healthcare Life Sciences) or anti-mouse IgG, HRP-linked F $(ab')_2$ fragment sheep (cat. no. NA9310; 1:10,000; GE Healthcare)] for 1 h at room temperature, and

an enhanced chemiluminescence western blot analysis system (Amersham; GE Healthcare) using a lumino image analyzer (LAS 4000 mini; Fujifilm). For re-blotting the membranes, the membranes were striped with WB Stripping Solution Strong (Nacalai Tesque, Inc.) for 1 h at 37˚C. Relative amounts of protein were calculated based on luminescence signals in each sample using Multigauge software (version 3.11; Fujifilm).

Hydroxyproline measurement. Hydroxyproline measurement was performed using 10 mg liver tissue that was homogenized in 100 μl distilled water prior to the addition of 100 μl 12 N hydrochloride acid. The samples were then hydrolyzed by incubation for 3 h at 120˚C. Following the addition of 5 mg activated charcoal and centrifugation at 10,000 x g for 5 min at 4˚C, the amount of hydroxyproline in the supernatants was measured using Hydroxyproline Assay kit (cat. no. STA675; Cell Biolabs Inc.).

Gelatin zymography. Frozen liver tissues were homogenized at 4˚C in buffer [50 mmol/l Tris-HCl (pH 7.6), 150 mmol/l NaCl, 0.1% SDS, 1% sodium deoxycholate, 1% NP-40 and 1% Triton-X 100], and the protein concentration was determined using a DC protein assay kit (Bio-Rad Laboratories, Inc.). Samples (50 μg protein) were loaded and resolved on a gelatin zymogram gel (10% SDS-PAGE gel with 0.1% gelatin). Gels were placed in 2.5% Triton X-100 solution for 30 min at 37˚C and then incubated for 18 h at 37˚C in enzyme activation buffer [50 mmol/l Tris-HCl (pH 7.5) with 5 mmol/l $CaCl_2$]. Gels were then stained at room temperature with 0.2% Coomassie blue R-250 (Nacalai Tesque, Inc.) for 30 min and de-stained at room temperature in 10% acetic acid and 20% methanol for 15 min, as described previously (15). Relative amounts of protein were calculated based on luminescence signals in each sample using Multigauge software (version 3.11; Fujifilm).

Serum analysis. The biochemical parameters (AST, ALT, total-protein, albumin and total-bilirubin) of serum samples were measured by Oriental Yeast Co., Ltd.

Statistical analysis. Data analyses were conducted using JMP Pro software v.13 (SAS Institute, Inc.). Differences between two groups were examined for statistical significance using an unpaired Student's t-test, and significant differences between multiple groups were determined using one-way ANOVA followed by a Tukey's post hoc test. All data are expressed as the mean ± SEM, and $P<0.05$ was considered to indicate a statistically significant difference.

Results

TGF-β signaling via TGF-β receptor type I kinase is inhibited by galunisertib in LX-2 cells. Galunisertib treatment of the human HSC line LX-2 dose-dependently decreased the levels of p-Smad2 and p-Smad3 independently of TGF-β1-induced signal activation, whereas galunisertib treatment did not affect Smad4 expression (Figs. 1A and S1). In the human hepatoblastoma HepG2 cell line, the level of p-Smad2 was similarly decreased by galunisertib treatment (Fig. S2A-D). Conversely, galunisertib did not inhibit phosphorylation of p38 MAPK or ERK1/2 in LX-2 cells (Figs. 1A and S1).

Effect of galunisertib on collagen and MMP synthesis, cell proliferation and angiogenesis. Galunisertib inhibited mRNA expression of collagen type I alpha 1 chain (COL1a1) in LX-2 cells in a dose-dependent manner (Fig. 1B). Conversely, galunisertib treatment dose-dependently restored MMP1 expression that was suppressed by TGF-β1 (Fig. 1C). Galunisertib treatment also dose-dependently inhibited LX-2 cell proliferation even in the presence of TGF-β1 stimulation (Fig. 1D). In addition, galunisertib treatment dose-dependently promoted HepG2 and HUVEC proliferation even in the presence of TGF-β1 stimulation (Fig. 1E and F). Furthermore, tube formation by HUVECs was promoted by galunisertib, as evidenced by the significant increase in the number of cavities observed following 2,000 nM galunisertib treatment (Fig. 1G and H).

Galunisertib treatment inhibits liver fibrosis progression in CCl_4-induced fibrotic liver. In gross appearance, the livers of mice in the vehicle-treated group had a dark red color, an irregular surface, and were more rigid compared with the intact group. Concomitantly, livers from the galunisertib-treated mice, particularly those in the high-dose group, were bright pink and had only a slightly irregular surface and little rigidity (Figs. 2A and S3). Galunisertib treatment increased the liver/ body weight (BW) ratio in a dose-dependent manner compared with the vehicle group [4.6±0.23% (vehicle) vs. 5.14±0.18% (low), 5.25±.33% (middle) and 6.11±0.27% (high); Fig. 2B]. In particular, the ratio was increased 1.7-fold in the high-dose group compared with the intact group (6.11±0.27 vs. 3.63±0.15%; Fig. 2B).

As demonstrated by the Mallory's Azan staining results, the extent of the fibrosis was attenuated remarkably in liver sections from mice treated with galunisertib compared with those treated with the vehicle (Fig. 3A). Semi-quantitative analysis indicated that the size of the fibrotic area was dose-dependently decreased with galunisertib treatment compared with vehicle group [1.13±0.11% (vehicle) vs. 0.91±0.06% (low), 0.55±0.08% (middle) and 0.33±.06% (high); Fig. 3B]. In addition, the galunisertib-treated livers exhibited fewer α-SMA-positive cells compared with the vehicle-treated livers (Fig. 3A). Semi-quantitative analysis of immunohistochemical staining intensity using anti-α-SMA antibody indicated that the sizes of the α-SMA-positive areas in mice treated with galunisertib were decreased in a dose-dependent manner compared with those in mice in the vehicle group [4.32±0.43% (vehicle) vs. 3.72±0.38% (low), 2.62±0.31% (middle) and 1.71±0.49% (high); Fig. 3C].

Hydroxyproline content, which is associated with the amount of collagen, in liver samples was increased ~2.1-fold by CCl_4 administration during the 8-week treatment period compared with the intact liver samples 849.7±52.1 (vehicle) vs. 408.9±19.4 (intact) (Fig. 3D). All galunisertib doses produced statistically significant decreases in the hydroxyproline content compared with that in the vehicle group, and the high-dose galunisertib treatment group exhibited a ~40% decrease in hydroxyproline content compared with the vehicle group [489.0±32.2 (high) vs. 849.7±52.1 μg/g (vehicle); Fig. 3D].

The results from the RT-qPCR demonstrated that there were no decreases in the expression levels of *Col1a1,* fibronectin 1 (*Fn1*) and actin alpha 2, smooth muscle (*Acta2*) mRNA after 8 weeks of CCl_4 treatment. The mRNA levels of these genes

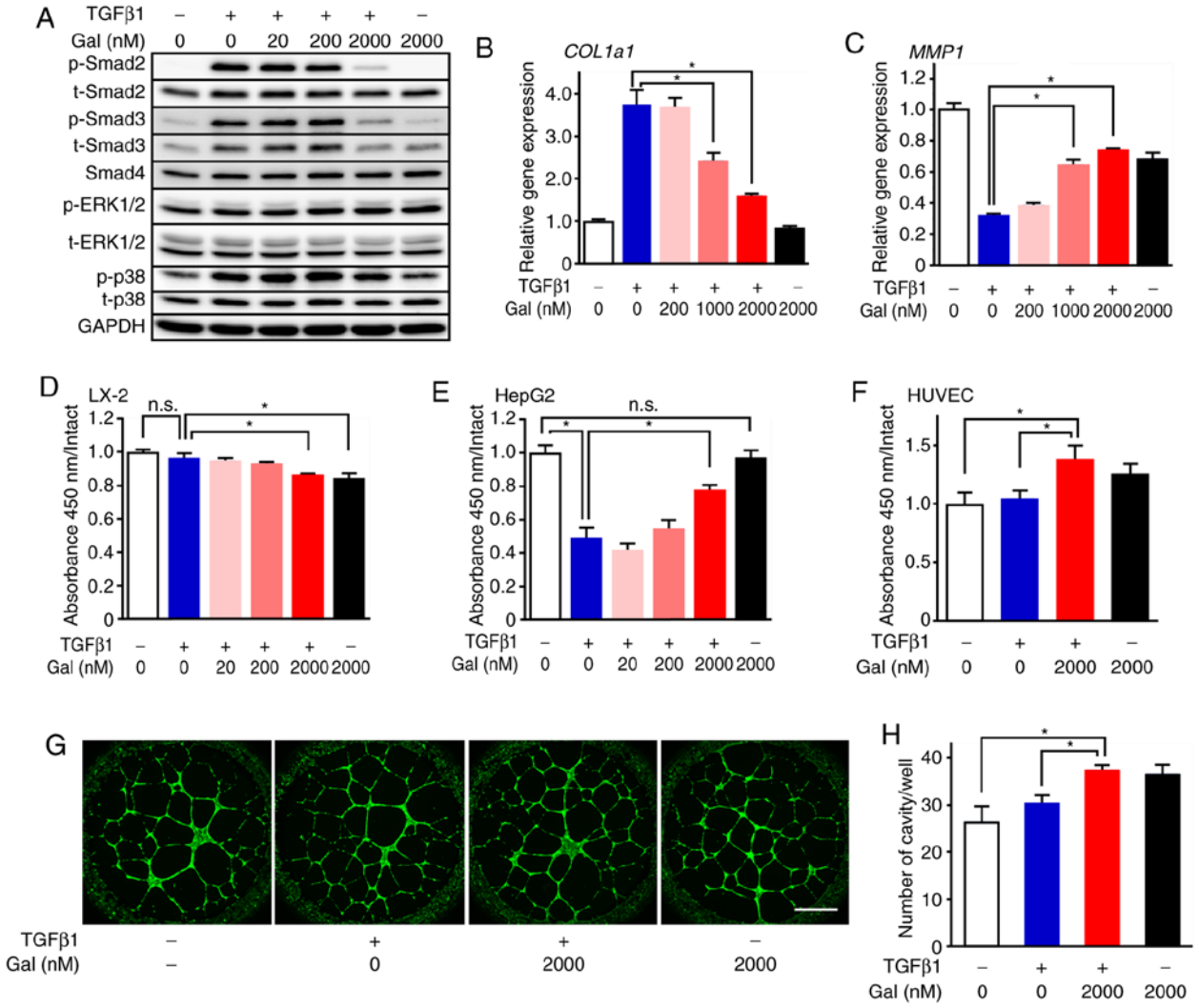

Figure 1. Anti-fibrotic and proliferative effects of galunisertib. (A) Effects of galunisertib on TGF-β signaling in LX-2 cells (n=4). p-Smad2, Smad3, p-Smad3, ERK1/2, p-ERK1/2, p38 MAPK, p-p38 and Smad4 protein expression levels were evaluated by western blot analysis. Galunisertib treatment dose-dependently decreased p-Smad2 and p-Smad3 expression levels, but not those of p-ERK1/2 and p-p38; (B and C) Effects of galunisertib on collagen and MMP production in LX-2 cells (n=4). (B) *COL1a1* and (C) *MMP1* mRNA expression levels were evaluated by reverse transcription-quantitative PCR. Galunisertib treatment dose-dependently inhibited and promoted *Col1a1* and *MMP1* mRNA expression, respectively. The effects of galunisertib on (D) LX-2, (E) HepG2 and (F) HUVEC cell proliferation (n=4-6). Galunisertib treatment inhibited LX-2 cell proliferation and promoted HepG2 and HUVEC proliferation even in the presence of TGF-β1 stimulation. (G and H) Effects of galunisertib in a tube formation assay with HUVEC (n=4). The number of the cavities significantly increased following galunisertib treatment. *P<0.05. Error bars represent the means ± SEM. Scale bar=1 mm. n.s., not significant; Gal, galunisertib; ERK, extracellular signal-regulated kinase; p-, phosphorylated; MMP, matrix metalloproteinase; COL1a1, collagen type I alpha 1 chain; TGF-β, transforming growth factor-β.

were also similar between mice treated with vehicle and all dosages of galunisertib (Fig. S4A-C).

Galunisertib treatment activated MMP in CCl_4-induced fibrotic liver. The MMP-1 expression level in the vehicle-treated group was significantly decreased compared with the level in the intact group, as shown by the data from the western blot analysis (Figs. 4A and S5) and RT-qPCR assays (Fig. S6A). In contrast to the *in vitro* results, the MMP-1 expression levels after 8 weeks of CCl_4 treatment were similar in samples from the galunisertib- and vehicle-treated livers. Semi-quantitative western blot analysis also revealed that, after 8 weeks of CCl_4 treatment, the expression levels of activated MMP-13 were similar in liver samples from galunisertib- and vehicle-treated mice (Figs. 4A and S5). Quantification of MMP-2 and MMP-9 expression by gelatin zymography indicated that the expression levels of pro- and active MMP-9, but not MMP-2, were significantly upregulated in galunisertib-treated livers compared with those in the vehicle-treated livers (Figs. 4B-F and S5D). Furthermore, RT-qPCR analysis indicated that the level of *Mmp9* mRNA expression after 8 weeks of CCl_4 treatment was significantly upregulated in livers from mice in the high-dose galunisertib group compared with those from the vehicle-treated group; however, there was no significant upregulation in expression levels of *Mmp1b*, *Mmp2*, *Mmp13* or TIMP metalloproteinase inhibitor 1 mRNA (Figs. 4G-J and S6C).

Galunisertib treatment promoted liver regeneration in CCl_4-induced fibrotic liver. In the galunisertib treatment groups, the percentage of PCNA-positive hepatocytes observed in the high-power fields increased in a dose-dependent manner (Fig. 5A). The number of PCNA-positive hepatocytes

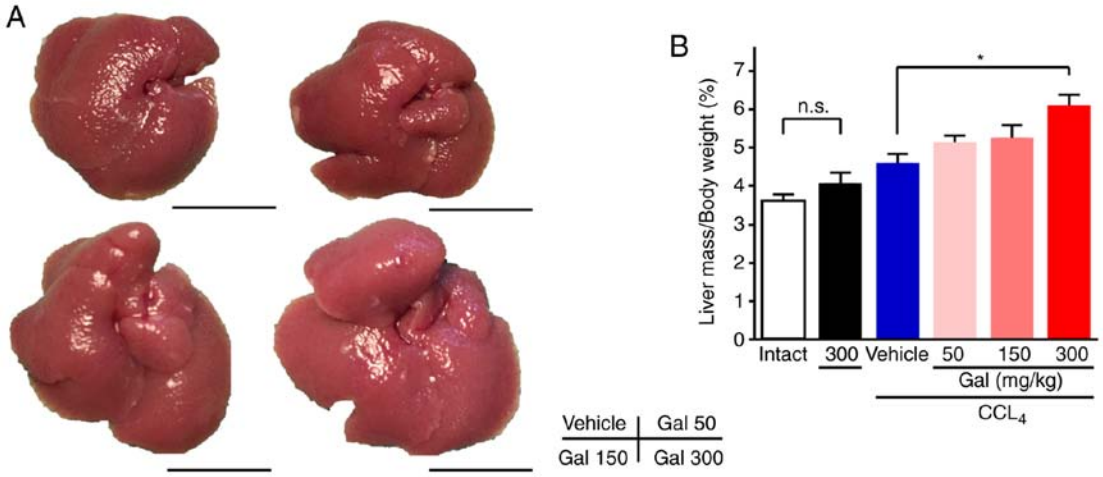

Figure 2. Gross appearance and liver/body weight ratio for mice treated with galunisertib. (A) Livers from CCl_4-treated mice exhibited a dark red color, an irregular surface and increased rigidity compared with livers from the intact group. Livers from the galunisertib-treated mice exhibited a bright pink color, a slightly irregular surface and minimal rigidity. (B) The ratio of liver/body weight for mice treated with galunisertib was dose-dependently and significantly increased compared with that for mice treated with vehicle. $^{*}P<0.05$. Error bars represent the means ± SEM. Scale bar=1 mm. Gal, galunisertib; CCl_4, carbon tetrachloride; Intact, no CCl_4 or galunisertib treatment; Vehicle, CCl_4-treated with no galunisertib treatment; Gal 50, livers from mice treated with low-dose galunisertib; Gal 150, treatment with middle-dose galunisertib; Gal 300, treatment with high-dose galunisertib; n.s., not significant.

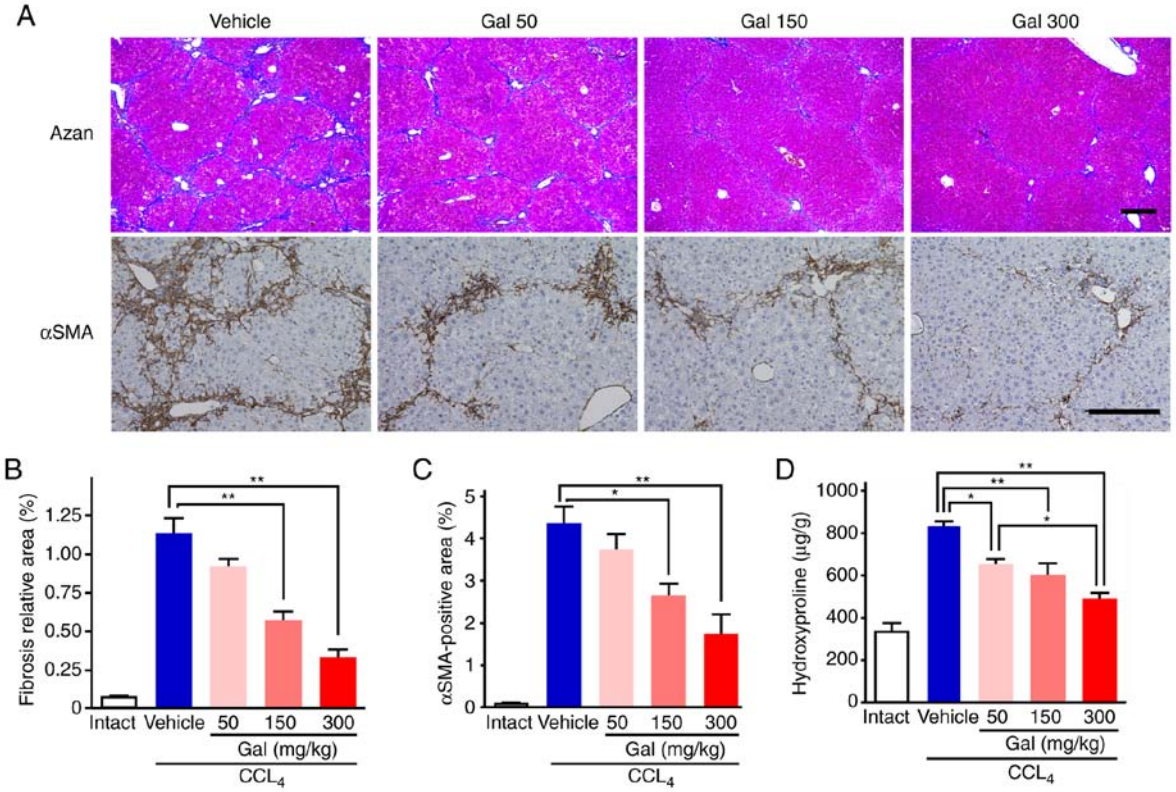

Figure 3. Histological assessment of cirrhotic livers from mice treated with galunisertib. (A) Mallory's Azan staining indicating that fibrosis was less remarkable in livers from mice treated with galunisertib compared with those treated with vehicle (upper panels). Galunisertib-treated livers exhibited fewer α-SMA-positive cells compared with vehicle-treated livers (lower panels). Scale bar=200 μm. (B) Semi-quantitative analysis of Mallory's Azan staining indicates that the percentage of fibrotic area was dose-dependently decreased in galunisertib-treated mice compared with vehicle-treated mice. (C) Semi-quantitative analysis of immunohistochemical staining area using an anti-α-SMA antibody indicated that the number of α-SMA-positive cells decreases dose-dependently with galunisertib treatment. (D) Hydroxyproline content in the liver. At all galunisertib doses, the hydroxyproline content significantly decreased compared with the vehicle group. $^{*}P<0.05$ and $^{**}P<0.01$. Error bars represent the means ± SEM. Gal, galunisertib; CCl_4, carbon tetrachloride; Intact, no CCl_4 or galunisertib treatment; Vehicle, CCl_4-treated with no galunisertib treatment; Gal 50, livers from mice treated with low-dose galunisertib; Gal 150, treatment with middle-dose galunisertib; Gal 300, treatment with high-dose galunisertib; α-SMA, α-smooth muscle actin.

increased around the portal vein, but not the central vein. In the high-dose galunisertib treatment group, the percentage of PCNA-positive hepatocytes increased by ~3-fold compared with that in the vehicle group [29.1±4.47 (high)

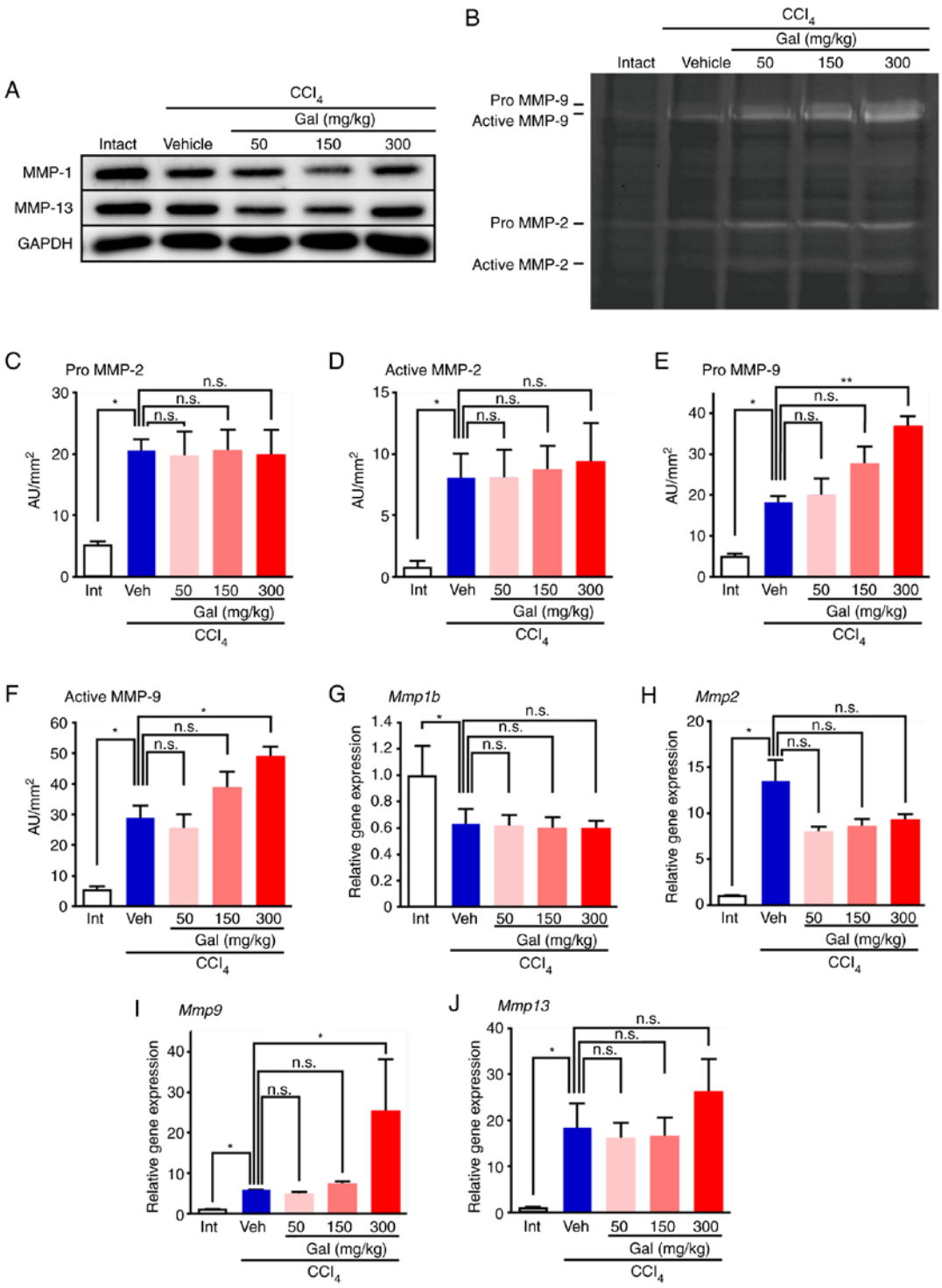

Figure 4. MMP expression and activity in cirrhotic livers from mice treated with galunisertib. (A) Western blot analysis data show that MMP-1 and MMP-13 expression levels were not increased in the livers from galunisertib-treated mice compared with vehicle-treated mice. (B) Gelatin zymography showing the active- and pro-forms of MMP-2 and MMP-9 after 8 weeks of CCl_4 treatment. The levels of the active and pro-forms of MMP-9 were significantly upregulated in livers from galunisertib-treated mice compared with those from vehicle-treated mice. (C-F) For semi-quantitative analyses, gelatin zymography bands of (C) pro-form of MMP-2, (D) active form of MMP-2, (E) pro-form of MMP-9 and (F) active form of MMP-9 were analyzed using image analysis software. (G-J) qRT-PCR analysis of *Mmp* mRNA expression. The levels of (G) *Mmp1b* and (H) *Mmp2* were similar between vehicle-treated mice and galunisertib-treated mice. (I) *Mmp9* mRNA expression was significantly upregulated in livers from mice treated with high-dose galunisertib compared with those from vehicle-treated livers. (J) *Mmp13* mRNA expression was similar between vehicle-treated mice and galunisertib-treated mice. For semi-quantitative analysis of gelatin zymography, 2 gels were assessed (n=4 in each group). The samples were derived from the same experiment and the gels were processed in parallel. $^{*}P<0.05$ and $^{**}P<0.01$. Error bars represent the means ± SEM. n.s., not significant; Gal, galunisertib; CCl_4, carbon tetrachloride; Intact or Int, no CCl_4 or galunisertib treatment; Vehicle or Veh, CCl_4 treatment without galunisertib; AU, arbitrary unit; MMP, matrix metalloproteinase.

vs. 10.2±2.71 (vehicle); Fig. 5B]. Western blot analysis of the levels of the PCNA protein in galunisertib-treated livers also demonstrated dose-dependent increases compared with the vehicle group (Figs. 5E and S7). By contrast, in the liver

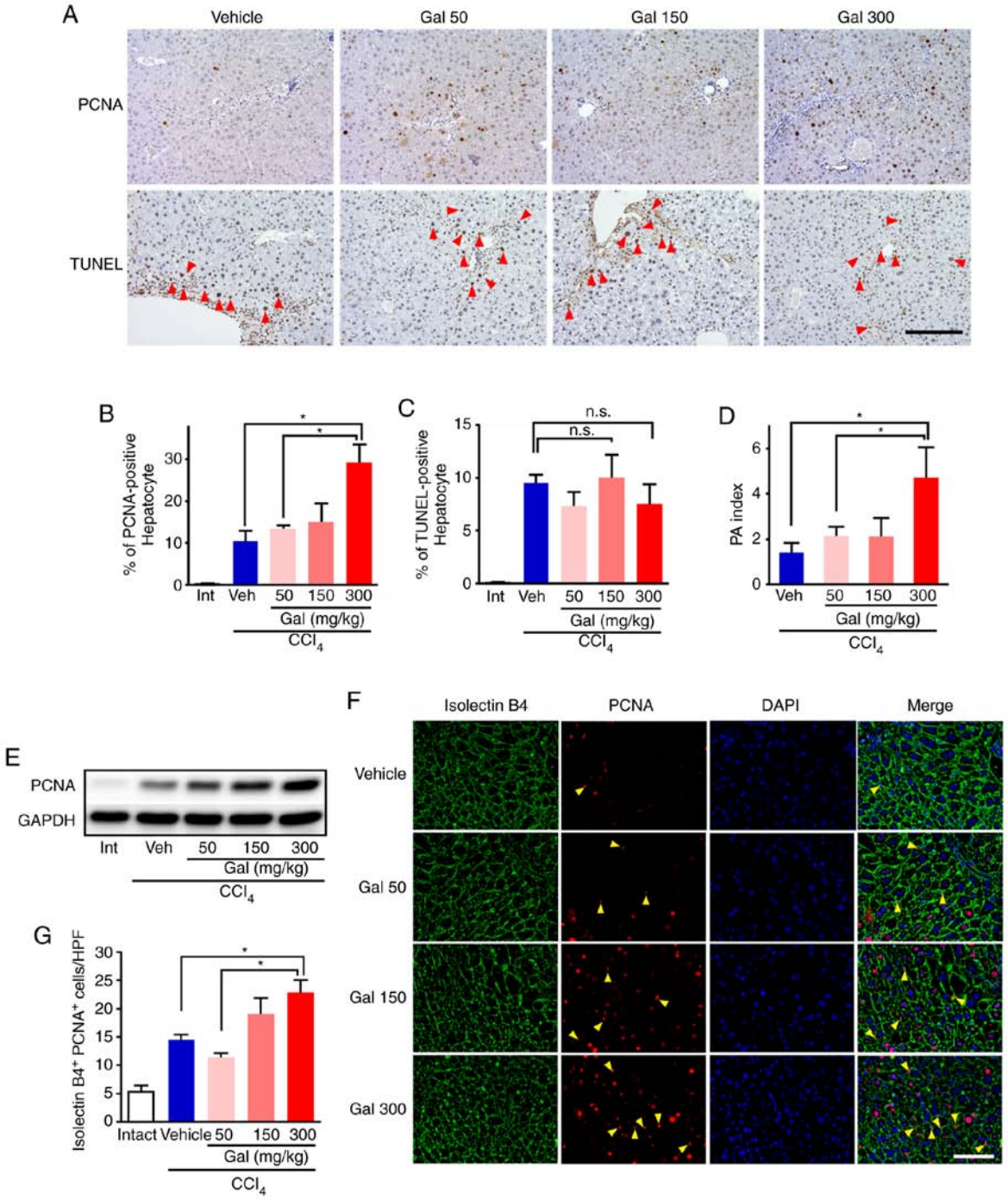

Figure 5. Galunisertib treatment accelerated proliferation of hepatocytes and endothelial cells. (A) In the galunisertib-treated mice, the numbers of PCNA-positive hepatocytes increased dose-dependently (upper panels). Concomitantly, the number of TUNEL-positive hepatocytes (arrowhead) was similar in galunisertib- and vehicle-treated mice (lower panels). Scale bar=200 μm; (B and C) For semi-quantitative analyses, (B) PCNA- and (C) TUNEL-positive hepatocytes were assessed using image analysis software. The percentage of PCNA-positive hepatocytes dose-dependently increased in livers from mice treated with galunisertib compared with those treated with vehicle, but the percentage of TUNEL-positive hepatocytes was similar in both groups. (D) The proliferation/apoptosis (PA) index was calculated by % PCNA-positive hepatocytes/% TUNEL-positive hepatocytes. In mice treated with high-dose galunisertib, the PA index was significantly increased compared with vehicle-treated mice. (E) PCNA protein expression levels in livers from galunisertib-treated mice exhibited dose-dependent increases. (F) In galunisertib-treated mice the number of $PCNA^+$ (red) and isolectin $B4^+$ (green) cells (arrowhead) increased in a dose-dependent manner. Scale bar=400 μm. (G) For semi-quantitative analyses, $PCNA^+$ isolectin $B4^+$ cells were assessed using image analysis software. In livers from galunisertib-treated mice, the number of $PCNA^+$ isolectin $B4^+$ cells was significantly increased compared with that for the vehicle-treated mice. $^*P<0.05$. Error bars represent the means ± SEM. Gal, galunisertib; CCl_4, carbon tetrachloride; Intact or Int, no CCl_4- or galunisertib treatment; Vehicle or Veh, CCl_4-treated without galunisertib treatment; Gal 50, low-dose galunisertib; Gal 150, middle-dose galunisertib; Gal 300, high-dose galunisertib; PCNA, proliferating cell nuclear antigen; TUNEL, terminal deoxynucleotidyl transferase mediated d-UTP nick end labeling; n.s., not significant.

samples from the galunisertib-treated groups, the percentage of TUNEL-positive hepatocytes and the number of cleaved caspase-3-positive hepatocytes observed in high power fields was similar to that for samples from vehicle-treated mice (Figs. 5C and S8). The proliferation/apoptosis (PA) index for hepatocytes from mice treated with high-dose galunisertib was

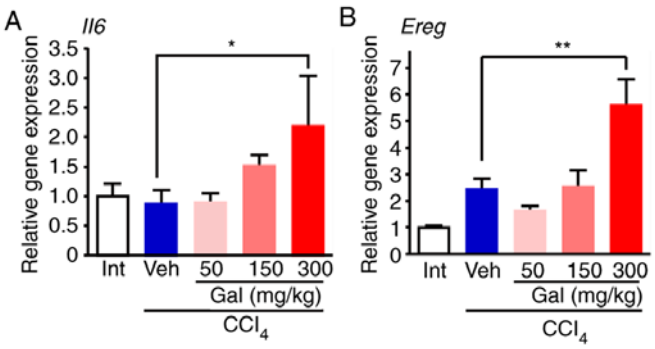

Figure 6. Expression of growth factors in cirrhotic livers from mice treated with galunisertib. (A and B) Reverse transcription-quantitative PCR analysis demonstrated that the *Il6* and *Ereg* expression levels were significantly increased in livers from mice treated with high-dose galunisertib compared with those from the vehicle-treated group. *P<0.05 and **P<0.01. Error bars represent the means ± SEM. Gal, galunisertib; CCl_4, carbon tetrachloride; Int, no CCl_4- or galunisertib treatment; Veh, CCl_4 treatment without galunisertib.

significantly increased compared with that from mice treated with the vehicle [4.70±1.36 (high) vs. 1.37±0.48 (vehicle); Fig. 5D]. To further evaluate the levels of cell proliferation and apoptosis, immunohistochemistry using an anti-p-AKT antibody was performed, but no signals were detected (data not shown). In the mice treated with high-dose galunisertib, the number of PCNA^{+}/isolectin B4^{+} double-positive liver endothelial cells was significantly increased after 8 weeks of CCl_4 treatment compared with those from the vehicle-treated mice [22.7±4.65 (high) vs. 14.4±2.61 (vehicle); Fig. 5F and G].

For the growth factors that are relevant to hepatocytes, the RT^2 profiler PCR array indicated that the expression levels of interleukin-6 (*Il6*), epiregulin (*Ereg*), fibroblast growth factor-7 (*Fgf7*), epithelial growth factor (*Egf*) and hepatocyte growth factor (*Hgf*) were upregulated in the livers from the high-dose galunisertib-treated group compared with the livers from the vehicle-treated group (Table SII). RT-qPCR analysis verified that *Il6* and *Ereg* expression levels were significantly increased in the livers from the high-dose galunisertib-treated group compared with the vehicle-treated group (Fig. 6A and B). Concomitantly, the RT-qPCR analysis of the mRNA expression levels of other growth factors, including *Fgf7, Egf, Hgf*, demonstrated that there were no significant differences between the experimental groups (Fig. S9A-C).

Toxic effects of galunisertib on liver function in mice with and without CCl_4 treatment. To evaluate the potential toxic effects of galunisertib, mice were treated with 300 mg/kg/day galunisertib (high-dose) for 4 weeks without CCl_4 administration and compared with the intact group. Although the serum levels of AST, ALT and total bilirubin between the two groups did not significantly change, those for total protein and albumin were significantly decreased in mice treated with high-dose galunisertib (Table I). Histologically, no significant differences were observed between the two groups (data not shown).

Next, the effects of galunisertib in fibrotic liver induced by CCl_4 treatment were investigated. No loss of BW was observed for any of the galunisertib treatment groups (data not shown). There were also no significant differences in the levels of serum total protein, AST, ALT and total bilirubin between the galunisertib-treated and vehicle groups, although the serum albumin level was significantly decreased in the high-dose group compared with the vehicle group (Table I).

Discussion

The present study showed that TGF-β1 treatment in LX-2 cells induced the phosphorylation of Smad2 and Smad3, and increased the expression of fibrosis genes. These changes could be inhibited by treatment with galunisertib at dosages that were in the range of plasma concentrations in human clinical trials (16,17). Similarly, it was shown in proliferating HepG2 cells that TGF-β1-induced Smad2 phosphorylation could be reversed by galunisertib. In addition, histology and measurement of liver hydroxyproline content were used to demonstrate that galunisertib dose-dependently suppressed liver fibrosis in mice with liver cirrhosis induced by CCl_4 treatment. These data strongly suggested that the TGF-β receptor type I kinase inhibitor galunisertib would be a feasible and effective anti-TGF-β therapy.

Galunisertib has been reported to affect the activity of TGF-β type-I receptors ALK4 and ALK5 and markedly inhibit the phosphorylation of Smad2 and Smad3 (10), and ERK1/2 phosphorylation (18). Conversely, TGF-β stimulation promotes phosphorylation of p38 MAPK independently of TGF-β receptor type-1 kinases (19). The present study examined the effects of galunisertib on intracellular signaling in HSC line LX-2. The results showed that galunisertib treatment of LX-2 cells markedly and dose-dependently decreased p-Smad2 and p-Smad3 expression levels, but did not affect p-p38 MAPK and p-ERK1/2 levels, even under activated conditions of TGF-β signaling. ERK1/2 was phosphorylated in the absence of TGF-β1 stimulation, which also did not promote ERK1/2 phosphorylation. These results suggested that phosphorylation of ERK1/2 is not regulated by TGF-β1 signaling in LX-2 cells. HSCs are fibrogenic cells that make major contributions to collagen accumulation during chronic liver disease. TGF-β/Smad3 signaling in LX-2 cells not only enhances the production of ECM, but also inhibits expression of MMP-1, which is the primary interstitial collagenase during fibrolysis (20). Indeed, the present study identified that galunisertib treatment inhibited the mRNA expression levels of *COL1a1* and increased those of *MMP1* in LX-2 cells in a dose-dependent manner. It was also shown that galunisertib treatment promoted cell proliferation of the human hepatoblastoma HepG2 cell line, even in the presence of TGF-β stimulation, which typically inhibits hepatocyte proliferation (5). In HCC tumorigenesis, TGF-β serves a dual role through tumor suppressive properties during the early disease stage and promotion of tumor progression at later stages of disease (21). Among HCC cell lines, HepG2, HuH7 and Hep3B cells belong to the early TGF-β signature subgroup of HCC models (22). As such, as an early TGF-β signature HCC cell line, HepG2 cells exhibit antiproliferative effects of TGF-β. Indeed, Serova *et al* (18) indicated that HepG2 cells exhibited the most marked TGF-β-mediated growth inhibition among 7 HCC cell lines. Together, these results suggested that galunisertib inhibits the canonical TGF-β signaling pathway *in vitro*.

Table I. Serum hepatobiliary parameters.

Groups	Total protein, g/dl	Albumin, g/dl	AST, IU/ml	ALT, IU/ml	Total bilirubin, mg/dl
Intact	5.38±0.05	3.75±0.03	45.00±2.36	21.25±0.85	0.07±0.00
High-dose without CCl_4	4.90±0.08[a]	3.28±0.03[a]	67.75±16.15	61.50±30.30	0.10±0.02
Vehicle	5.40±0.04	3.54±0.05	130.43±41.55	124.71±8.63	0.16±0.02
Low-dose	5.54±0.04	3.59±0.05	120.00±40.71	112.71±12.22	0.16±0.04
Middle-dose	5.34±0.06	3.47±0.08	220.43±59.18	160.14±32.19	0.19±0.02
High-dose	5.28±0.09	3.28±0.09[b]	255.75±62.71	203.25±66.17	0.17±0.00

[a]P<0.01 compared with Intact group. [b]P<0.05 compared with Vehicle group. Data are represented as the mean ± SEM. CCl_4, carbon tetrachloride; Intact, no CCl_4 or galunisertib treatment; Vehicle, CCl_4-treated with no galunisertib treatment; Low-dose, treatment with low-dose galunisertib; Middle-dose, treatment with middle-dose galunisertib; High-dose, treatment with high-dose galunisertib.

Fibrolysis mechanisms involve the inhibition of ECM production and/or increase of collagenolytic activity (4). HSCs serve a central role in liver fibrogenesis (4). In mice with CCl_4-induced cirrhosis, the present study showed that galunisertib treatment dose-dependently decreased the percentage of liver fibrotic areas and α-SMA-positive areas, as well as the hydroxyproline content, compared with the vehicle-treated mice. α-SMA is a well-known marker of activated HSCs and increased ECM production is mediated by activated HSCs (23). However, the present study identified that none of the administered doses of galunisertib significantly decreased *Col1a1, Fn1* and *Acta2* mRNA expression levels compared with the vehicle group. This result could be attributed to the short (0.3 h) half-life of galunisertib in mice (10) and could be affected by the sample collection time. Furthermore, it was identified that the activity of MMP-9 was increased in a dose-dependent fashion following galunisertib administration. Following activation by MMP-2, MMP-9 degrades fibronectin and type-IV collagen, which are both major structural components of basement membranes (24). The results of the present study are consistent with those of a study by Hammad *et al* (25), which demonstrated that the amount of ECM/stromal components fibronectin and laminin-332, as well as the activity of the carcinogenic β-catenin pathway, is remarkably decreased in galunisertib-treated Abcb4Ko mice, another mouse model of chronic liver disease. Together, these data indicate that galunisertib administration can promote fibrolysis. Meanwhile, MMP-1 in humans and MMP-13 in mice have been shown to serve as the major MMPs that degrade interstitial collagens (26-28). The present study showed that galunisertib treatment dose-dependently increased MMP-1 expression in LX-2 cells under TGF-β1 stimulation, but that MMP-13 levels were similar in livers from galunisertib-treated and vehicle-treated mice. Therefore, in mice, the fibrolytic action of galunisertib appears to be mediated through the degradation of collagen, which is a primary component of basement membranes.

Notably, enhanced regeneration of hepatocytes was detected by immunohistochemistry and western blot analysis using an anti-PCNA antibody. This result is consistent with that of Karkampouna *et al* (29), who reported that the co-administration of LY364947, an inhibitor that targets the TGF-β type-I receptor kinase ALK5, with CCl_4 resulted in enhanced hepatic regeneration, as measured by changes in PCNA levels. In addition, TGF-β regulates the G1 to S phase transition of hepatocytes, but intact TGF-β-mediated signaling is not required to inhibit liver regeneration, as compensatory increases in activin A signaling can occur (30).

Galunisertib is in Phase II trials for treatment of liver cancer (NCT01246986 and NCT02178358). Therefore, the present study explored the effect of clinical stage on the activity of galunisertib as a TGF-β pathway inhibitor. The *in vivo* antifibrotic and regenerative efficacy of galunisertib using a dose of 75 mg/kg administered twice daily by oral gavage was evaluated. This dosing schedule was defined by the PK/PD profile, as described previously (11). Ongoing clinical trials involving galunisertib are testing doses of 160 or 300 mg/day (BID) (NCT01246986 and NCT02178358). Therefore, the low- and moderate-doses of galunisertib used in the present study correspond to clinically relevant doses undergoing testing in human clinical trials. However, 300 mg/kg/day galunisertib is considered to be a toxic dose, and it has been already reported that continuous administration of galunisertib at 300 mg/kg/day for 3 months causes side effects (31).

The present study identified that, in comparison with the untreated mice, 300 mg/kg/day galunisertib was associated with a significant increase in liver weight as well as a significant decrease in albumin levels; the ALT and AST levels were also increased, although not significantly, when compared with the untreated mice. Concomitantly, albumin levels were also significantly decreased in mice treated with 300 mg/kg/day galunisertib that were not exposed to CCl_4 as compared with the intact group. To demonstrate that the observed hepatomegaly was not hepatotoxic, the association between cell proliferation and apoptosis during progression of CCl_4-induced liver fibrosis was examined. In liver samples from mice treated with 300 mg/kg/day galunisertib, the percentage of TUNEL-positive hepatocytes did not increase, but the PA index was significantly increased compared with the hepatocytes from the vehicle-treated mice. These results suggest that the increase of liver weight may be attributed to an promotion of the hepatocyte proliferation. Previous studies indicated that liver weight was either maintained or increased following inhibition of TGF-β and Activin A in a partial hepatectomy model and in normal livers (32,33). Galunisertib inhibits the activity of both ALK4 and ALK5, but may also inhibit the activin A signaling pathway (11,34). Inhibition of

both TGF-β/ALK5 and Activin A/ALK4 signaling pathways may be associated with the increased liver weight observed in mice treated with galunisertib.

The effects of ALK5 inhibitors on angiogenesis have recently been reported (35). In the present study, the effects of galunisertib on liver fibrosis associated with angiogenesis were evaluated using a cell proliferation and tube formation assay with HUVEC and a mouse model of angiogenesis. It was identified that galunisertib treatment promoted angiogenesis by HUVEC regardless of TGF-β stimulation. This result is consistent with that of Liu *et al* (35), who showed that a combination of galunisertib and VEGF more potently induced angiogenesis compared with VEGF alone. In the *in vitro* study, both the proliferation and tube formation assays using HUVEC were performed in the presence of several growth factors including VEGF. In addition, our previous studies suggested that the VEGF levels in liver tissue are elevated in the CCl_4-induced cirrhosis model (15,36). Taken together, these results indicate that galunisertib treatment promoted angiogenesis in the CCl_4-induced cirrhosis model.

Another explanation for galunisertib-mediated resolution of fibrosis and promotion of hepatic regeneration is an increase in growth factor expression following galunisertib administration. The results of the present study showed that galunisertib treatment significantly upregulated the mRNA expression levels of both *Il6* and *Ereg* in liver tissues. IL-6 is a cytokine that is primarily produced by T cells and macrophages, and is also involved in inflammation and the development of certain immune system diseases, in addition to its ability to promote hepatocyte proliferation (37). TGF-β also has an immunosuppressive effect. Therefore, inhibition of the TGF-β pathway by galunisertib may affect IL-6 secretion by immune cells. Epiregulin is expressed by the *Ereg* gene in Thy-1-positive cells, for example mesenchymal cells or liver progenitor cells, and has been reported to contribute to liver regeneration (38). Increases in epiregulin expression may in turn increase the number of hepatic progenitor cells, although the results of promoting hepatocyte proliferation support that galunisertib-mediated inhibition of the TGF-β pathway may be the main driver of increased proliferation of mature hepatocytes. These possibilities require further investigation.

In terms of side effects, CCl_4-treated mice that were administered galunisertib exhibited an increased liver/BW ratio, whereas mice that received only galunisertib and no CCl_4 showed no significant change in this ratio (data not shown). These results appear reflect hepatic regeneration; however, atypical increases in liver weight is known to be a transient effect that can arise due to the inhibition of the TGF-β and Activin A signaling pathways (33). In the biochemical analysis of serum samples, the levels of total protein and albumin were significantly decreased by high-dose galunisertib treatment without CCl_4 administration, in comparison with the intact group. The cause of this effect is not clear, but no obvious histological differences were observed between the two groups.

In conclusion, the present study demonstrated that anti-TGF-β therapy using galunisertib ameliorated liver fibrosis by decreasing the number of activated HSCs and increasing the activity of MMP-9, as well as enhancing hepatic regeneration by elevating growth factor levels, including *Il6* and *Ereg*. Phase II clinical trials of galunisertib for treatment of HCC are currently ongoing. The majority of patients with HCC also have liver cirrhosis, and thus determination of both the tolerability and safety of galunisertib, as well as its ability to induce fibrolysis and liver regeneration, is important. The results of the present study may provide insights into the development of novel therapies for liver cirrhosis.

Acknowledgements

The authors thank Ms. Mari Hagihara (Division of Gastroenterology, Department of Medicine, School of Medicine, Kurume University, Kurume, Japan) for technical assistance in the preparation of tissue sections and Ms. Masako Hayakawa (Liver Cancer Research Division, Research Center for Innovative Cancer Therapy, Kurume University, Kurume, Japan) for excellent technical assistance.

Funding

The present study was supported in part by a grant from the Kurume University Millennium Box Foundation for the Promotion of Science and by the Medical Care Education Research Foundation.

Availability of data and materials

The datasets used and/or analyzed during the current study are available from the corresponding author on reasonable request.

Authors' contributions

TN, HK and TTo made substantial contributions to the conception and design of the study. AM and TN conceived and designed the study, performed the experiments and wrote the manuscript. MA and HI performed the experiments. TS, TTa and HS performed the data analysis. All authors edited and reviewed the final manuscript.

Ethics approval and consent to participate

All experiments were approved by the Ethics Review Committee for Animal Experimentation of the Kurume University School of Medicine and were performed in accordance with Eli Lilly and company animal care and use requirements for animal researchers and suppliers.

Patient consent for publication

Not applicable.

Competing interests

The authors declare that they have no competing interests.

References

1. Schuppan D and Afdhal NH: Liver cirrhosis. Lancet 371: 838-851, 2008.
2. Fattovich G, Stroffolini T, Zagni I and Donato F: Hepatocellular carcinoma in cirrhosis: Incidence and risk factors. Gastroenterology 127 (5 Suppl 1): S35-S50, 2004.

3. Tarao K, Nozaki A, Ikeda T, Sato A, Komatsu H, Komatsu T, Taguri M and Tanaka K: Real impact of liver cirrhosis on the development of hepatocellular carcinoma in various liver diseases-meta-analytic assessment. Cancer Med 8: 1054-1065, 2019.
4. Tsuchida T and Friedman SL: Mechanisms of hepatic stellate cell activation. Nat Rev Gastroenterol Hepatol 14: 397-411, 2017.
5. Nguyen LN, Furuya MH, Wolfraim LA, Nguyen AP, Holdren MS, Campbell JS, Knight B, Yeoh GC, Fausto N and Parks WT: Transforming growth factor-beta differentially regulates oval cell and hepatocyte proliferation. Hepatology 45: 31-41, 2007.
6. Nakamura T, Sakata R, Ueno T, Sata M and Ueno H: Inhibition of transforming growth factor beta prevents progression of liver fibrosis and enhances hepatocyte regeneration in dimethylnitrosamine-treated rats. Hepatology 32: 247-255, 2000.
7. Ueno H, Sakamoto T, Nakamura T, Qi Z, Astuchi N, Takeshita A, Shimizu K and Ohashi H: A soluble transforming growth factor beta receptor expressed in muscle prevents liver fibrogenesis and dysfunction in rats. Hum Gene Ther 11: 33-42, 2000.
8. Nakamura T, Ueno T, Sakamoto M, Sakata R, Torimura T, Hashimoto O, Ueno H and Sata M: Suppression of transforming growth factor-beta results in upregulation of transcription of regeneration factors after chronic liver injury. J Hepatol 41: 974-982, 2004.
9. Yingling JM, Blanchard KL and Sawyer JS: Development of TGF-beta signalling inhibitors for cancer therapy. Nat Rev Drug Discov 3: 1011-1022, 2004.
10. Herbertz S, Sawyer JS, Stauber AJ, Gueorguieva I, Driscoll KE, Estrem ST, Cleverly AL, Desaiah D, Guba SC, Benhadji KA, *et al*: Clinical development of galunisertib (LY2157299 monohydrate), a small molecule inhibitor of transforming growth factor-beta signaling pathway. Drug Des Devel Ther 9: 4479-4499, 2015.
11. Yingling JM, McMillen WT, Yan L, Huang H, Sawyer JS, Graff J, Clawson DK, Britt KS, Anderson BD, Beight DW, *et al*: Preclinical assessment of galunisertib (LY2157299 monohydrate), a first-in-class transforming growth factor-β receptor type I inhibitor. Oncotarget 9: 6659-6677, 2017.
12. Ikeda M, Morimoto M, Tajimi M, Inoue K, Benhadji KA, Lahn MMF and Sakai D: A phase Ib study of transforming growth factor-beta receptor I inhibitor galunisertib in combination with sorafenib in Japanese patients with unresectable hepatocellular carcinoma. Invest New Drugs 37: 118-126, 2019.
13. Luangmonkong T, Suriguga S, Bigaeva E, Boersema M, Oosterhuis D, de Jong KP, Schuppan D, Mutsaers HAM and Olinga P: Evaluating the antifibrotic potency of galunisertib in a human ex vivo model of liver fibrosis. Br J Pharmacol 174: 3107-3117, 2017.
14. Livak KJ and Schmittgen TD: Analysis of relative gene expression data using real-time quantitative PCR and the 2(-Delta Delta C(T)) method. Methods 25: 402-408, 2001.
15. Nakamura T, Torimura T, Sakamoto M, Hashimoto O, Taniguchi E, Inoue K, Sakata R, Kumashiro R, Murohara T, Ueno T and Sata M: Significance and therapeutic potential of endothelial progenitor cell transplantation in a cirrhotic liver rat model. Gastroenterology 133: 91-107.e101, 2007.
16. Gueorguieva I, Cleverly AL, Stauber A, Sada Pillay N, Rodon JA, Miles CP, Yingling JM and Lahn MM: Defining a therapeutic window for the novel TGF-β inhibitor LY2157299 monohydrate based on a pharmacokinetic/pharmacodynamic model. Br J Clin Pharmacol 77: 796-807, 2014.
17. Faivre S, Santoro A, Kelley RK, Gane E, Costentin CE, Gueorguieva I, Smith C, Cleverly A, Lahn MM, Raymond E, *et al*: Novel transforming growth factor beta receptor I kinase inhibitor galunisertib (LY2157299) in advanced hepatocellular carcinoma. Liver Int 39: 1468-1477, 2019.
18. Serova M, Tijeras-Raballand A, Dos Santos C, Albuquerque M, Paradis V, Neuzillet C, Benhadji KA, Raymond E, Faivre S and de Gramont A: Effects of TGF beta signalling inhibition with galunisertib (LY2157299) in hepatocellular carcinoma models and in ex vivo whole tumor tissue samples from patients. Oncotarget 6: 21614-21627, 2015.
19. Heldin CH and Moustakas A: Signaling receptors for TGF-β family members. Cold Spring Harb Perspect Biol 8: a022053, 2016.
20. Yuan W and Varga J: Transforming growth factor-beta repression of matrix metalloproteinase-1 in dermal fibroblasts involves Smad3. J Biol Chem 276: 38502-38510, 2001.
21. Breuhahn K, Longerich T and Schirmacher P: Dysregulation of growth factor signaling in human hepatocellular carcinoma. Oncogene 25: 3787-3800, 2006.
22. Coulouarn C, Factor VM and Thorgeirsson SS: Transforming growth factor-beta gene expression signature in mouse hepatocytes predicts clinical outcome in human cancer. Hepatology 47: 2059-2067, 2008.
23. Bataller R and Brenner DA: Liver fibrosis. J Clin Invest 115: 209-218, 2005.
24. Ram M, Sherer Y and Shoenfeld Y: Matrix metalloproteinase-9 and autoimmune diseases. J Clin Immunol 26: 299-307, 2006.
25. Hammad S, Cavalcanti E, Werle J, Caruso ML, Dropmann A, Ignazzi A, Ebert MP, Dooley S and Giannelli G: Galunisertib modifies the liver fibrotic composition in the Abcb4Ko mouse model. Arch Toxicol 92: 2297-2309, 2018.
26. Iimuro Y, Nishio T, Morimoto T, Nitta T, Stefanovic B, Choi SK, Brenner DA and Yamaoka Y: Delivery of matrix metalloproteinase-1 attenuates established liver fibrosis in the rat. Gastroenterology 124: 445-458, 2003.
27. Endo H, Niioka M, Sugioka Y, Itoh J, Kameyama K, Okazaki I, Ala-Aho R, Kähäri VM and Watanabe T: Matrix metalloproteinase-13 promotes recovery from experimental liver cirrhosis in rats. Pathobiology 78: 239-252, 2011.
28. Fallowfield JA, Mizuno M, Kendall TJ, Constandinou CM, Benyon RC, Duffield JS and Iredale JP: Scar-associated macrophages are a major source of hepatic matrix metalloproteinase-13 and facilitate the resolution of murine hepatic fibrosis. J Immunol 178: 5288-5295, 2007.
29. Karkampouna S, Goumans MJ, Ten Dijke P, Dooley S and Kruithof-de Julio M: Inhibition of TGFβ type I receptor activity facilitates liver regeneration upon acute CCl_4 intoxication in mice. Arch Toxicol 90: 347-357, 2016.
30. Oe S, Lemmer ER, Conner EA, Factor VM, Levéen P, Larsson J, Karlsson S and Thorgeirsson SS: Intact signaling by transforming growth factor beta is not required for termination of liver regeneration in mice. Hepatology 40: 1098-1105, 2004.
31. Stauber AJ, Credille KM, Truex LL, Ehlhardt WJ and Young JK: Nonclinical safety evaluation of a transforming growth factor β receptor I kinase inhibitor in fischer 344 rats and beagle dogs. J Clin Pract 4: 196, 2014.
32. Kogure K, Omata W, Kanzaki M, Zhang YQ, Yasuda H, Mine T and Kojima I: A single intraportal administration of follistatin accelerates liver regeneration in partially hepatectomized rats. Gastroenterology 108: 1136-1142, 1995.
33. Ichikawa T, Zhang YQ, Kogure K, Hasegawa Y, Takagi H, Mori M and Kojima I: Transforming growth factor beta and activin tonically inhibit DNA synthesis in the rat liver. Hepatology 34: 918-925, 2001.
34. Fields SZ, Parshad S, Anne M, Raftopoulos H, Alexander MJ, Sherman ML, Laadem A, Sung V and Terpos E: Activin receptor antagonists for cancer-related anemia and bone disease. Expert Opin Investig Drugs 22: 87-101, 2013.
35. Liu Z, Kobayashi K, van Dinther M, van Heiningen SH, Valdimarsdottir G, van Laar T, Scharpfenecker M, Löwik CW, Goumans MJ, Ten Dijke P and Pardali E: VEGF and inhibitors of TGFbeta type-I receptor kinase synergistically promote blood-vessel formation by inducing alpha5-integrin expression. J Cell Sci 122: 3294-3302, 2009.
36. Nakamura T, Tsutsumi V, Torimura T, Naitou M, Iwamoto H, Masuda H, Hashimoto O, Koga H, Abe M, Ii M, *et al*: Human peripheral blood CD34-positive cells enhance therapeutic regeneration of chronically injured liver in nude rats. J Cell Physiol 227: 1538-1552, 2012.
37. Tao Y, Wang M, Chen E and Tang H: Liver regeneration: Analysis of the main relevant signaling molecules. Mediators Inflamm 2017: 4256352, 2017.
38. Tomita K, Haga H, Mizuno K, Katsumi T, Sato C, Okumoto K, Nishise Y, Watanabe H, Saito T and Ueno Y: Epiregulin promotes the emergence and proliferation of adult liver progenitor cells. Am J Physiol Gastrointest Liver Physiol 307: G50-G57, 2014.